PNAS

Supplementary Information for
The effectiveness of COVID-19 testing and contact tracing in a US city

Xutong Wang[1], Zhanwei Du[1, 2, 3], Emily James[4], Spencer J Fox[1], Michael Lachmann[5], Lauren Ancel Meyers[1, 5*], Darlene Bhavnani[6*]

[*]Darlene Bhavnani, Lauren Ancel Meyers

Email: Darlene.Bhavnani@austin.utexas.edu, laurenmeyers@austin.utexas.edu

This PDF file includes:

Supplementary text
Figures S1 to S3.5
Tables S1.1 to S2.2
SI References

Supplementary Information Text

Section 1. COVID-19 Epidemic Model Structure and Parameters

Model structure

The model structure is diagrammed in Figure S1 and described in the equations below. For each age and risk group, we build a separate set of compartments to model the transitions between the states: susceptible (*S*), exposed that are undetectable (E^U), exposed that are detectable (E^D), exposed that are isolated (E^Q), symptomatic infectious that are undetectable (I^{YU}), symptomatic infectious that are detectable (I^{YD}), symptomatic infectious that are isolated (I^{YQ}), asymptomatic infectious that are undetectable (I^{AU}), asymptomatic infectious that are detectable (I^{AD}), asymptomatic infectious that are isolated (I^{AQ}), symptomatic infectious that are hospitalized (I^H), recovered (*R*), and deceased (*D*). The symbols S, E^U, E^D, E^Q, I^{YU}, I^{YD}, I^{YQ}, I^{AU}, I^{AD}, I^{AQ}, I^H, R, and D denote the number of people in that state in the given age/risk group and the total size of the age/risk group is $N = S + E^U + E^D + E^Q + I^{YU} + I^{YD} + I^{YQ} + I^{AU} + I^{AD} + I^{AQ} + I^H + R + D$. The model for individuals in age group *a* and risk group *r* is given by:

$$\frac{dS_{a,r}}{dt} = -S_{a,r}\sum_{i\in A}\sum_{j\in K}\Big(\big(I_{i,j}^{YU} + I_{i,j}^{YD} + \kappa I_{i,j}^{YQ}\big)\omega^Y + \big(I_{i,j}^{AU} + I_{i,j}^{AD} + \kappa I_{i,j}^{AQ}\big)\omega^A + \big(E_{i,j}^{U} + E_{i,j}^{D} + \kappa E_{i,j}^{Q}\big)\omega^E\Big)\beta\phi_{a,i}/N_i$$

$$\frac{dE_{a,r}^U}{dt} = (1-\delta^E)S_{a,r}\sum_{i\in A}\sum_{j\in K}\Big(\big(I_{i,j}^{YU} + I_{i,j}^{YD} + \kappa I_{i,j}^{YQ}\big)\omega^Y + \big(I_{i,j}^{AU} + I_{i,j}^{AD} + \kappa I_{i,j}^{AQ}\big)\omega^A + \big(E_{i,j}^{U} + E_{i,j}^{D} + \kappa E_{i,j}^{Q}\big)\omega^E\Big)\beta\phi_{a,i}/N_i - \sigma E_{a,r}^U$$

$$\frac{dE_{a,r}^D}{dt} = \delta^E S_{a,r}\sum_{i\in A}\sum_{j\in K}\Big(\big(I_{i,j}^{YU} + I_{i,j}^{YD} + \kappa I_{i,j}^{YQ}\big)\omega^Y + \big(I_{i,j}^{AU} + I_{i,j}^{AD} + \kappa I_{i,j}^{AQ}\big)\omega^A + \big(E_{i,j}^{U} + E_{i,j}^{D} + \kappa E_{i,j}^{Q}\big)\omega^E\Big)\beta\phi_{a,i}/N_i - \sigma E_{a,r}^D$$

$$\frac{dE_{a,r}^Q}{dt} = \rho^E E_{a,r}^D - \sigma E_{a,r}^Q$$

$$\frac{dI_{a,r}^{AU}}{dt} = (1-\delta^A)(1-\tau)\sigma E_{a,r}^U - \gamma^{AU} I_{a,r}^{AU}$$

$$\frac{dI_{a,r}^{AD}}{dt} = \delta^A(1-\tau)\sigma E_{a,r}^U + (1-\tau)\sigma E_{a,j}^D - \rho^A I_{a,r}^{AD}$$

$$\frac{dI_{a,r}^{AQ}}{dt} = (1-\tau)\sigma E_{a,j}^Q + \rho^A I_{a,r}^{AD} - \gamma^{AQ} I_{a,r}^{AQ}$$

$$\frac{dI_{a,r}^{YU}}{dt} = (1-\delta^Y)\tau\sigma E_{a,r}^U - (1-\pi^U)\gamma^{YU} I_{a,r}^{YU} - \pi^U\eta I_{a,r}^{YU}$$

$$\frac{dI_{a,r}^{YD}}{dt} = \delta^Y\tau\sigma E_{a,r}^U + \tau\sigma E_{a,r}^D - (1-\pi^D)\rho^Y I_{a,r}^{YD} - \pi^D\eta I_{a,r}^{YD}$$

$$\frac{dI_{a,r}^{YQ}}{dt} = \tau\sigma E_{a,r}^Q + (1-\pi^D)\rho^Y I_{a,r}^{YD} - \gamma^{YQ} I_{a,r}^{YQ}$$

$$\frac{dI_{a,r}^{H}}{dt} = \pi^U\eta I_{a,r}^{YU} + \pi^D\eta I_{a,r}^{YD} - (1-\nu)\gamma^H I_{a,r}^{H} - \nu\mu I_{a,r}^{H}$$

$$\frac{dR_{a,r}}{dt} = \gamma^{AU} I_{a,r}^{AU} + \gamma^{AQ} I_{a,r}^{AQ} + (1-\pi^U)\gamma^{YU} I_{a,r}^{YU} + \gamma^{YQ} I_{a,r}^{YQ} + (1-\nu)\gamma^H I_{a,r}^{H}$$

$$\frac{dD_{a,r}}{dt} = \nu\mu I_{a,r}^{H}$$

where *A* and *K* are all possible age and risk groups, ω^A, ω^Y, ω^E are the relative infectiousness of the $I^{A\cdot}$, $I^{Y\cdot}$, $E^{\cdot}$ compartments, respectively, hospitalized individuals (I^H) are assumed to be isolated and thus effectively non-infectious, β is transmission rate, $\phi_{a,i}$ is the mixing rate between

age group a, $i \in A$, $\delta^A, \delta^Y, \delta^E$ are detection rate of the $I^{A\cdot}$, $I^{Y\cdot}$, $E^{\cdot}$ compartments, respectively, ρ^A, ρ^Y, ρ^E are rate that I^{AD}, I^{YD}, E^D compartments move to isolation, respectively, $\gamma^{AU}, \gamma^{AQ}, \gamma^{YU}, \gamma^{YQ}, \gamma^H$ are the recovery rates for the $I^{AU}, I^{AQ}, I^{YU}, I^{YQ}, I^H$ compartments, respectively, σ is the exposed rate, τ is the symptomatic ratio, π^U, π^D is the proportion of symptomatic individuals requiring hospitalization for I^{YU}, I^{YD} compartments, η is rate at which hospitalized cases enter the hospital following symptom onset, ν is mortality rate for hospitalized cases, and μ is rate at which terminal patients die.

We model stochastic transitions between compartments using the τ-leap method (1, 2) with key parameters given in Table S1. Assuming that the events at each time-step are independent and do not impact the underlying transition rates, the numbers of each type of event should follow Poisson distributions with means equal to the rate parameters. We thus simulate the model according to the following equations:

$$
\begin{aligned}
S_{a,r}(t+1) - S_{a,r}(t) &= -P_1 \\
E^U_{a,r}(t+1) - E^U_{a,r}(t) &= (1-\delta^E)P_1 - P_2 \\
E^D_{a,r}(t+1) - E^D_{a,r}(t) &= \delta^E P_1 - P_3 - P_4 \\
E^Q_{a,r}(t+1) - E^Q_{a,r}(t) &= P_4 - P_5 \\
I^{AU}_{a,r}(t+1) - I^{AU}_{a,r}(t) &= (1-\delta^A)(1-\tau)P_2 - P_6 \\
I^{YU}_{a,r}(t+1) - I^{YU}_{a,r}(t) &= (1-\delta^Y)\tau P_2 - P_7 - P_8 \\
I^{AD}_{a,r}(t+1) - I^{AD}_{a,r}(t) &= \delta^A(1-\tau)P_2 + (1-\tau)P_3 - P_9 \\
I^{YD}_{a,r}(t+1) - I^{YD}_{a,r}(t) &= \delta^Y \tau P_2 + \tau P_3 - P_{10} - P_{11} \\
I^{AQ}_{a,r}(t+1) - I^{AQ}_{a,r}(t) &= (1-\tau)P_5 + P_9 - P_{12} \\
I^{YQ}_{a,r}(t+1) - I^{YQ}_{a,r}(t) &= \tau P_5 + P_{10} - P_{13} \\
I^{H}_{a,r}(t+1) - I^{H}_{a,r}(t) &= P_8 + P_{11} - P_{14} - P_{15} \\
D_{a,r}(t+1) - D_{a,r}(t) &= P_{14} \\
R_{a,r}(t+1) - R_{a,r}(t) &= P_6 + P_7 + P_{12} + P_{13} + P_{15},
\end{aligned}
$$

with

$$
\begin{aligned}
P_1 &\sim Pois\left(S_{a,r}(t)F_{a,r}(t)\right) \\
P_2 &\sim Pois\left(\sigma E^U_{a,r}(t)\right) \\
P_3 &\sim Pois\left(\sigma E^D_{a,r}(t)\right) \\
P_4 &\sim Pois\left(\rho^E E^D_{a,r}(t)\right) \\
P_5 &\sim Pois\left(\sigma E^Q_{a,r}(t)\right) \\
P_6 &\sim Pois\left(\gamma^{AU} I^{AU}(t)\right) \\
P_7 &\sim Pois\left((1-\pi^U)\gamma^{YU} I^{YU}(t)\right) \\
P_8 &\sim Pois\left(\pi^U \eta I^{YU}(t)\right) \\
P_9 &\sim Pois\left(\rho^A I^{AD}_{a,r}(t)\right) \\
P_{10} &\sim Pois\left((1-\pi^D)\rho^Y I^{YD}_{a,r}(t)\right) \\
P_{11} &\sim Pois\left(\pi^D \eta I^{YD}_{a,r}(t)\right) \\
P_{12} &\sim Pois\left(\gamma^{AQ} I^{AQ}(t)\right) \\
P_{13} &\sim Pois\left(\gamma^{YQ} I^{YQ}(t)\right) \\
P_{14} &\sim Pois\left(\nu\mu I^{H}(t)\right) \\
P_{15} &\sim Pois\left((1-\nu)\gamma^{H} I^{H}(t)\right)
\end{aligned}
$$

and where $F_{a,r}$ denotes the force of infection for individuals in age group a and risk group r and is given by:

$$F_{a,r}(t) = \sum_{i \in A} \sum_{j \in K} \left(\left(I_{i,j}^{YU} + I_{i,j}^{YD} + \kappa I_{i,j}^{YQ} \right) \omega^{Y} + \left(I_{i,j}^{AU} + I_{i,j}^{AD} + \kappa I_{i,j}^{AQ} \right) \omega^{A} + \left(E_{i,j}^{U} + E_{i,j}^{D} + \kappa E_{i,j}^{Q} \right) \omega^{E} \right) \beta \phi_{a,i} / N_i$$

Testing and tracing parameter derivation

Let , $\delta^{A}, \delta^{Y}, \delta^{E}$denote detection rate of the $I^{A\cdot}$, $I^{Y\cdot}$, $E^{\cdot}$ compartments, respectively, $\rho^{A}, \rho^{Y}, \rho^{E}$be rate that I^{AD}, I^{YD}, E^{D} compartments move to isolation, respectively. Let *yd* be the symptomatic case detection ratio and *trs* be the probability of a contact is successfully reached.

- Let hc be the number of days that a symptomatic individual seek healthcare after symptom onset, then $(\rho^{Y})^{-1} = hc$
- Let d be the number of days from infectee's exposure to being traced, and *tr* be the delay in contact tracing, then $d \sim Triangular(tr, \sigma^{-1} + (\rho^{Y})^{-1} - E[i] + tr, \sigma^{-1} + (\rho^{Y})^{-1})$, where $E[i]$ is the expected days from infector's infection to infectee's exposure. $E[i] = \sum_{i=0}^{\sigma^{-1}+(\rho^{Y})^{-1}} i \cdot Pr[detected\ on\ day\ i](1 - Pr[detected\ before\ day\ i])$
- $Pr[infected\ by\ symptomatic\ people] = \frac{(1-P)\omega^{Y}}{\omega^{A}+\omega^{Y}} + P(1-\tau)$where *P* is the proportion of pre-symptomatic infection
- $Pr[detectable\ through\ contact\ tracing]$=$Pr[infected\ by\ symptomatic\ people] \cdot yd \cdot trs$
- $\delta^{E} = Pr[d < \sigma^{-1}] \cdot Pr[detectable\ through\ contact\ tracing]$ and $\delta^{A} = Pr[d > \sigma^{-1}] \cdot Pr[detectable\ through\ contact\ tracing]$
- $(\rho^{E})^{-1} = E[d < \sigma^{-1}] = \sigma^{-1} + (\rho^{Y})^{-1} + tr - E[i > (\rho^{Y})^{-1} + tr]$
- $(\rho^{A})^{-1} = E[d > \sigma^{-1}] - \sigma^{-1} = (\rho^{Y})^{-1} + tr - E[i < (\rho^{Y})^{-1} + tr]$

Cumulative infectivity calculation

Let I be the number of days that a contact was infected when the individual was traced and $I \in [tr,\ tr + (\rho^{Y})^{-1} + \sigma^{-1}]$, then $Pr\ [I = i\ ] = Pr\ [infected\ on\ day\ i]\ \cdot (1 - Pr\ [infected\ before\ day\ i]\ )$.
Let C_i be the cumulative infectivity that an infected individual has on day i. Let $f(x)$ indicate the infectivity curve (3), then $C_i = \frac{\int_{-\sigma^{-1}+i}^{-\sigma^{-1}+i+1} f(x)dx}{\int_{-\sigma^{-1}}^{(\gamma^{Y})^{-1}} f(x)dx}$. Therefore, the mean cumulative infectivity of an infected contact $\underline{C} = \sum_i C_i \cdot Pr[I = i]$.

Initial Conditions

Initial conditions were derived using a COVID-19 healthcare forecasting model that we developed in a partnership with the city of Austin and used to provide daily transmission and healthcare projections on a public dashboard (4). The forecasting model is almost identical to the model in this study. Specifically, it is an expanded stochastic SEIR model with eight disease progression compartments, including symptomatic, pre-symptomatic, asymptomatic patients, and hospitalization. The population is divided into five age groups, with different rates of contacts within and between age groups, a high-risk category with each age group, and age- and risk-specific rates of hospitalization. The demographic, health and mixing parameters are identical to those assumed in this study.

To make daily dashboard projections, we incorporate anonymized local mobility data from SafeGraph (5) into transmission rate. We assume published estimates for all disease progression parameters and calibrate the remaining unknown states and parameters to local COVID-19 hospital admissions and discharge data using iterated filtering made available through the POMP R package (6). The result of the statistical inference is posterior densities for parameters governing the impact of mobility on transmission and the reporting process of hospitalization data,

and for hidden states of the model including the number of infected individuals. Additional details are provided in ref. (7).

To obtain initial conditions for this study, we used the states in the fitted model based on data through November 7, 2020, as given in Table S1.8.

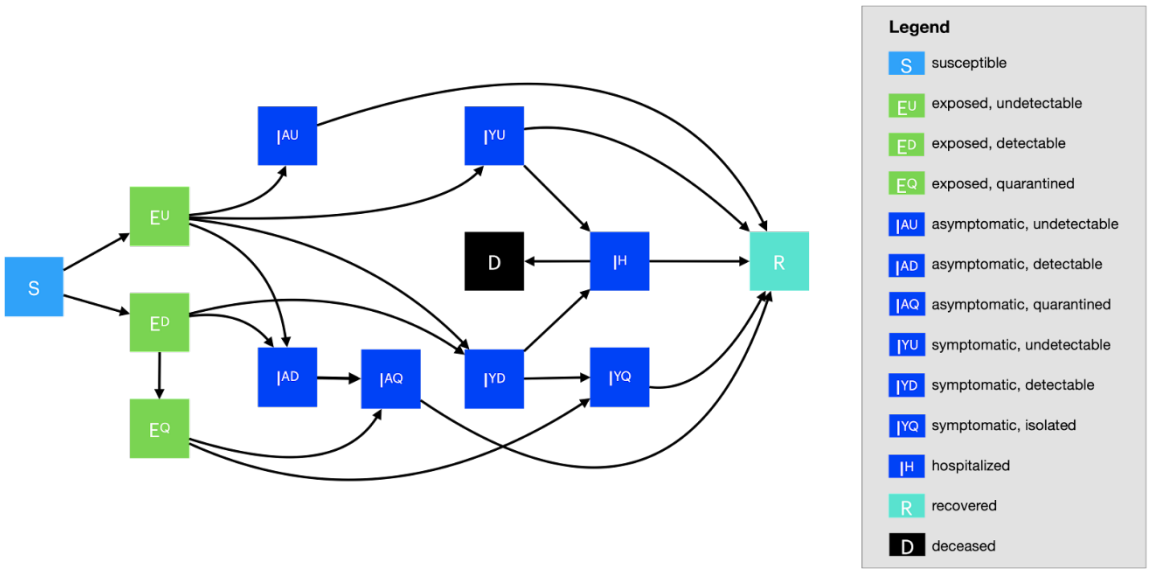

Figure S1. Compartmental model of COVID-19 transmission in a US city. Each subgroup (defined by age and risk) is modeled with a separate set of compartments. Upon infection, susceptible individuals (S) progress to either exposed that are undetectable (E^U) or exposed that are detectable (E^D). Part of the exposed individuals that are undetectable will progress to either symptomatic infectious (I^{YU}) or asymptomatic infectious (I^{AU}). The remaining exposed individuals that are undetectable in the incubation period will become detectable in the infectious period, so progress to detectable asymptomatic (I^{AD}) or symptomatic (I^{YD}). Exposed individuals that are detectable (E^D) will either isolate (E^Q) then progress to isolated asymptomatic (I^{AQ}) or isolated symptomatic (I^{YQ}), or progress to detectable asymptomatic or symptomatic then to asymptomatic isolated or symptomatic isolated. All asymptomatic cases eventually progress to a recovered class where they remain protected from future infection (R); symptomatic cases are either hospitalized (I^H) or recover. Mortality (D) varies by age group and risk group and is assumed to be preceded by hospitalization.

Table S1.1. Initial conditions, school closures and social distancing policies

Variable	Settings
Initial day of simulation	11/8/2020
Initial infection number in locations	Based on estimates for Austin, Texas, given Table S1.8 (4)
Age-specific and day-specific contact rates[a]	Home, work, other and school matrices provided in Tables S1.4-S1.7 Typical weekday = home + work + other + school Weekends and holiday weekdays = home + other Weekdays during non-holiday school breaks = home + work + other
School calendar	Austin Independent School District calendar (2019-2020, 2020-2021) (8)

[a] We assume the age-specific contact rates given in ref. (9), which takes the contact numbers estimated through diary-based POLYMOD study in Europe (10) and extrapolates to the United States. The values in Tables S1.4-S1.7 are the assumed daily contacts between each pair of age groups at home, school, work, and all other places, respectively. These contact matrices are used to adjust the transmission rate between age groups. The accuracy of the contact matrices is limited by (i) possible biases with the original diary-based study (10), (ii) assumptions made when projecting the original study to the US (9), and (iii) impacts of COVID-19 policies and perceptions on daily contact patterns. Beginning in March 2020, many employees began working from home and public schools transitioned to remote instruction. As a result, contact rates outside the home would have decreased, while contacts within the home would have increased. Our model assumes that work and school contacts occur only on weekdays while home and 'other' contacts occur on all days. We model reductions in transmission during lock down periods by fitting our transmission rate parameter to local hospitalization data, rather than directly modifying the contact matrices. Thus, we may overestimate the proportion of transmission events that occur among children during periods of school closure, but capture the overall force of infection fairly accurately. Furthermore, local COVID-19 restrictions had relaxed by September 2020, before the study period began, and contact patterns rebounded towards pre-pandemic patterns.

Table S1.2. Epidemiological parameters. Values given as five-element vectors are age-stratified with values corresponding to 0-4, 5-17, 18-49, 50-64, 65+ year age groups, respectively.

Parameters	Best guess values	Source
R_0	0.95, 1.2	Assumption
β: baseline transmission rate	0.013, 0.016	Derived from next generation matrix based on R_0 (11)
Serial interval (days)	5.8	(12)
γ^A: recovery rate on asymptomatic compartment	Equal to γ^Y	
γ^Y: recovery rate on symptomatic non-treated compartment	$\frac{1}{\gamma^Y} \sim Triangular(3, 4, 5)$	(12)
τ: symptomatic proportion (%)	57	(13)
σ: exposed rate	Incubation period $\frac{1}{\sigma} \sim Triangular(4.2, 5.2, 6.2)$	(12)
P: proportion of pre-symptomatic (%)	44	(12)
ω^E: relative infectiousness of infectious individuals in compartment E	$\omega^E = \frac{\left(\frac{YHR}{\eta} + \frac{1-YHR}{\gamma^Y}\right)\omega^Y \sigma P}{1-P}$	
ω^A: relative infectiousness of infectious individuals in compartment I^A	0.67	(12, 14)
IFR: infected fatality ratio, age specific (%)	Overall: [0.0016, 0.00495, 0.08428, 1.00011, 3.37149] Low risk: [0.00092, 0.00218, 0.03388, 0.25197, 0.64402] High risk: [0.00917, 0.02179, 0.33878, 2.51968, 6.44015]	Age adjusted from Verity et al. (15)

YFR: symptomatic fatality ratio, age specific (%)	Overall: [0.00281, 0.00868, 0.14785, 1.75458, 5.9149] Low risk: [0.00161, 0.00382, 0.05943, 0.44205, 1.12985] High risk: [0.01608, 0.03823, 0.59434, 4.42048, 11.29851]	$YFR = \frac{IFR}{\tau}$
h: high-risk proportion, age specific (%)	[8.2825, 14.1121, 16.5298, 32.9912, 47.0568]	Estimated using 2015-2016 Behavioral Risk Factor Surveillance System (BRFSS) data with multilevel regression and poststratification using CDC's list of conditions that may increase the risk of serious complications from influenza (16–18)
rr: relative risk for high risk people compared to low risk in their age group	10	Assumption
hc: days that a symptomatic individual seek healthcare after symptom onset	2	Based on local data
yd: symptomatic case detection ratio	40%, 80%	Assumption
trs: probability of a contact is successfully reached	25%, 50%, 75%	Assumption
Contact reduction for an individual in isolation	0.95	Assumption
Contact reduction for an individual in quarantine	0.75	Assumption

Table S1.3. Hospitalization parameters

Parameters	Value	Source
γ^H: recovery rate in hospitalized compartment	$\frac{1}{\gamma^H} \sim Triangular(9.4,10.7,12.8)$	Austin admissions and discharge data (Avg=10.96. 95% CI = 9.37 to 12.76) (19, 20)
YHR: symptomatic case hospitalization rate (%)	Overall: [0.07018, 0.07018, 4.73526, 16.32983, 25.54183] Low risk: [0.04021, 0.03091, 1.90348, 4.11413, 4.87895] High risk: [0.40205, 0.30913, 19.03482, 41.14127, 48.78947]	Age adjusted from Verity et al. (15)
π: rate of symptomatic individuals go to hospital, age-specific	$\pi = \frac{\gamma^Y \cdot YHR}{\eta + (\gamma^Y - \eta)YHR}$	
η: rate from symptom onset to hospitalized	0.1695	5.9 day average from symptom onset to hospital admission Tindale et al. (21)
μ: rate from hospitalized to death	$\frac{1}{\mu} \sim Triangular(5.2,8.1,10.1)$	Austin admissions and discharge data (Avg=7.8, 95% CI = 5.21 to 10.09) (19, 20)
HFR: hospitalized fatality ratio, age specific (%)	[4, 12.365, 3.122, 10.745, 23.158]	$HFR = \frac{YFR}{YHR}$
ν: death rate on hospitalized individuals, age specific	$\nu = \frac{\gamma^H HFR}{\mu + (\gamma^H - \mu)HFR}$	

Table S1.4. Home contact matrix (daily number contacts by age group at home)

	0-4y	5-17y	18-49y	50-64y	65y+
0-4y	0.5	0.9	2.0	0.1	0.0
5-17y	0.2	1.7	1.9	0.2	0.0
18-49y	0.2	0.9	1.7	0.2	0.0
50-64y	0.2	0.7	1.2	1.0	0.1
65y+	0.1	0.7	1.0	0.3	0.6

Table S1.5. School contact matrix (daily number contacts by age group at school)

	0-4y	**5-17y**	**18-49y**	**50-64y**	**65y+**
0-4y	1.0	0.5	0.4	0.1	0.0
5-17y	0.2	3.7	0.9	0.1	0.0
18-49y	0.0	0.7	0.8	0.0	0.0
50-64y	0.1	0.8	0.5	0.1	0.0
65y+	0.0	0.0	0.1	0.0	0.0

Table S1.6. Work contact matrix (daily number contacts by age group at work)

	0-4y	5-17y	18-49y	50-64y	65y+
0-4y	0.0	0.0	0.0	0.0	0.0
5-17y	0.0	0.1	0.4	0.0	0.0
18-49y	0.0	0.2	4.5	0.8	0.0
50-64y	0.0	0.1	2.8	0.9	0.0
65y+	0.0	0.0	0.1	0.0	0.0

Table S1.7. Others contact matrix (daily number contacts by age group at other locations)

	0-4y	5-17y	18-49y	50-64y	65y+
0-4y	0.7	0.7	1.8	0.6	0.3
5-17y	0.2	2.6	2.1	0.4	0.2
18-49y	0.1	0.7	3.3	0.6	0.2
50-64y	0.1	0.3	2.2	1.1	0.4
65y+	0.0	0.2	1.3	0.8	0.6

Table S1.8. Initial states of model compartments. Values indicate the number of individuals in each age-risk group compartment at the start of the simulations.

Age	Risk	S	E	I^A	I^Y	I^H	R	D
0-4 yr	High	8809	12	3	5	0	524	0
	Low	121035	168.5	55	73	0	7190	0
5-17 yr	High	33884	75.5	24	33	0	3418	0
	Low	296425	674	210	279	0	29580	1
18-49 yr	High	142443	286	92	140	35	13158	26
	Low	834952	1720	555	746	21	77836	16
50-64 yr	High	100333	177	53	87	42	7262	255
	Low	231158	394.5	122	171	9	17369.5	57
65+ yr	High	100100.5	82	24	43	20	3261	236
	Low	127788	105	36	51	2	4485	31

Section 2. Estimation of age-stratified proportion of population at high-risk for COVID-19 complications

We estimate age-specific proportions of the population at high risk of complications from COVID-19 based on data for Austin, TX and Round-Rock, TX from the CDC's 500 cities project (Figure S2) (22). We assume that high risk conditions for COVID-19 are the same as those specified for influenza by the CDC (16). The CDC's 500 cities project provides city-specific estimates of prevalence for several of these conditions among adults.(23) The estimates were obtained from the 2015-2016 Behavioral Risk Factor Surveillance System (BRFSS) data using a small-area estimation methodology called multi-level regression and poststratification (17, 18). It links geocoded health surveys to high spatial resolution population demographic and socioeconomic data (18).

Estimating high-risk proportions for adults. To estimate the proportion of adults at high risk for complications, we use the CDC's 500 cities data, as well as data on the prevalence of HIV/AIDS, obesity and pregnancy among adults (Table S2.1).

The CDC 500 cities dataset includes the prevalence of each condition on its own, rather than the prevalence of multiple conditions (e.g., dyads or triads). Thus, we use separate co-morbidity estimates to determine overlap. Reference about chronic conditions (24) gives US estimates for the proportion of the adult population with 0, 1 or 2+ chronic conditions, per age group. Using this and the 500 cities data we can estimate the proportion of the population pHR in each age group in each city with at least one chronic condition listed in the CDC 500 cities data (Table S2.1) putting them at high-risk for flu complications.

HIV: We use the data from table 20a in CDC HIV surveillance report (25) to estimate the population in each risk group living with HIV in the US (last column, 2015 data). Assuming independence between HIV and other chronic conditions, we increase the proportion of the population at high-risk for influenza to account for individuals with HIV but no other underlying conditions.

Morbid obesity: A BMI over 40kg/m^2 indicates morbid obesity and is considered high risk for influenza. The 500 Cities Project reports the prevalence of obese people in each city with BMI over 30kg/m^2 (not necessarily morbid obesity). We use the data from table 1 in Sturm and Hattori (26) to estimate the proportion of people with BMI>30 that actually have BMI>40 (across the US); we then apply this to the 500 Cities obesity data to estimate the proportion of people who are morbidly obese in each city. Table 1 of Morgan et al. (27) suggests that 51.2% of morbidly obese adults have at least one other high risk chronic condition, and update our high-risk population estimates accordingly to account for overlap.

Pregnancy: We separately estimate the number of pregnant women in each age group and each city, following the methodology in CDC reproductive health report (28). We assume independence between any of the high-risk factors and pregnancy, and further assume that half the population are women.

Estimating high-risk proportions for children. Since the 500 Cities Project only reports data for adults 18 years and older, we take a different approach to estimating the proportion of children at high risk for severe influenza. The two most prevalent risk factors for children are asthma and obesity; we also account for childhood diabetes, HIV and cancer.

From Miller et al. (29), we obtain national estimates of chronic conditions in children. For asthma, we assume that variation among cities will be similar for children and adults. Thus, we use the relative prevalence of asthma in adults to scale our estimates for children in each city. The prevalence of HIV and cancer in children are taken from CDC HIV surveillance report (25) and cancer research report (30), respectively.

We first estimate the proportion of children having either asthma, diabetes, cancer or HIV (assuming no overlap in these conditions). We estimate city-level morbid obesity in children using the estimated morbid obesity in adults multiplied by a national constant ratio for each age group estimated from Hales et al. (31), this ratio represents the prevalence in morbid obesity in children given the one observed in adults. From Morgan et al. (27), we estimate that 25% of morbidly obese children have another high-risk condition and adjust our final estimates accordingly.

Resulting estimates. We compare our estimates for the Austin-Round Rock Metropolitan Area to published national-level estimates (32) of the proportion of each age group with underlying high risk conditions (Table S2.2). The biggest difference is observed in older adults, with Austin having a lower proportion at risk for complications for COVID-19 than the national average; for 25-39 year-old the high risk proportion is slightly higher than the national average.

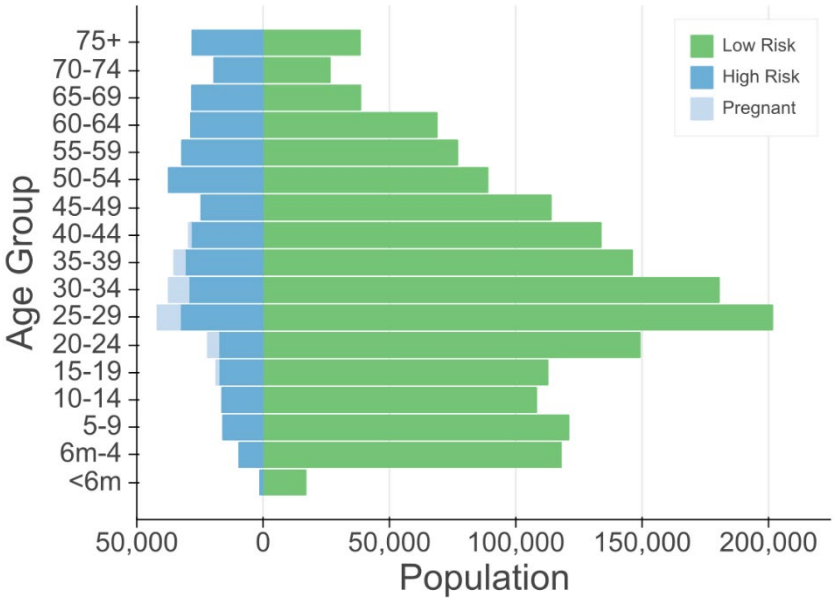

Figure S2. Demographic and risk composition of the Austin-Round Rock population. Bars indicate age-specific population sizes, separated by low risk, high risk, and pregnant. High risk is defined as individuals with cancer, chronic kidney disease, COPD, heart disease, stroke, asthma, diabetes, HIV/AIDS, and morbid obesity, as estimated from the CDC 500 Cities Project (22), reported HIV prevalence (25) and reported morbid obesity prevalence (26, 27), corrected for multiple conditions. The population of pregnant women is derived using the CDC's method combining fertility, abortion and fetal loss rates (33–35).

Table S2.1. High-risk conditions for influenza and data sources for prevalence estimation

Condition	Data source
Cancer (except skin)	CDC 500 cities (22)
Chronic kidney disease	CDC 500 cities (22)
COPD	CDC 500 cities (22)
Coronary heart disease	CDC 500 cities (22)
Stroke	CDC 500 cities (22)
Asthma	CDC 500 cities (22)
Diabetes	CDC 500 cities (22)
HIV/AIDS	CDC HIV Surveillance report (25)
Obesity	CDC 500 cities complemented with Sturm and Hattori(26) and Morgan et al. (27)
Pregnancy	National Vital Statistics Reports (33) and abortion data (34)

Table S2.2. Comparison between published national estimates and Austin-Round Rock MSA estimates of the percent of the population at high-risk of influenza/COVID-19 complications

Age Group	National estimates (31)	Austin (excluding pregnancy)	Pregnant women (proportion of age group)
0 to 6 months	NA	6.8	-
6 months to 4 years	6.8	7.4	-
5 to 9 years	11.7	11.6	-
10 to 14 years	11.7	13.0	-
15 to 19 years	11.8	13.3	1.7
20 to 24 years	12.4	10.3	5.1
25 to 34 years	15.7	13.5	7.8
35 to 39 years	15.7	17.0	5.1
40 to 44 years	15.7	17.4	1.2
45 to 49 years	15.7	17.7	-
50 to 54 years	30.6	29.6	-
55 to 60 years	30.6	29.5	-
60 to 64 years	30.6	29.3	-
65 to 69 years	47.0	42.2	-
70 to 74 years	47.0	42.2	-
75 years and older	47.0	42.2	-

Section 3. Sensitivity analyses and additional figures with respect to hospitalizations and deaths

Sensitivity analysis with respect to compliance with isolation and quarantine

Our base scenarios assume that isolation and quarantine reduce contacts by 95% and 75%, respectively. Here, we consider a lower compliance scenario in which these reductions are 75% and 50%, respectively. The expected effectiveness of the test-trace-isolate program decreases, but the relative performance of the various strategies does not change (Figure S3.1).

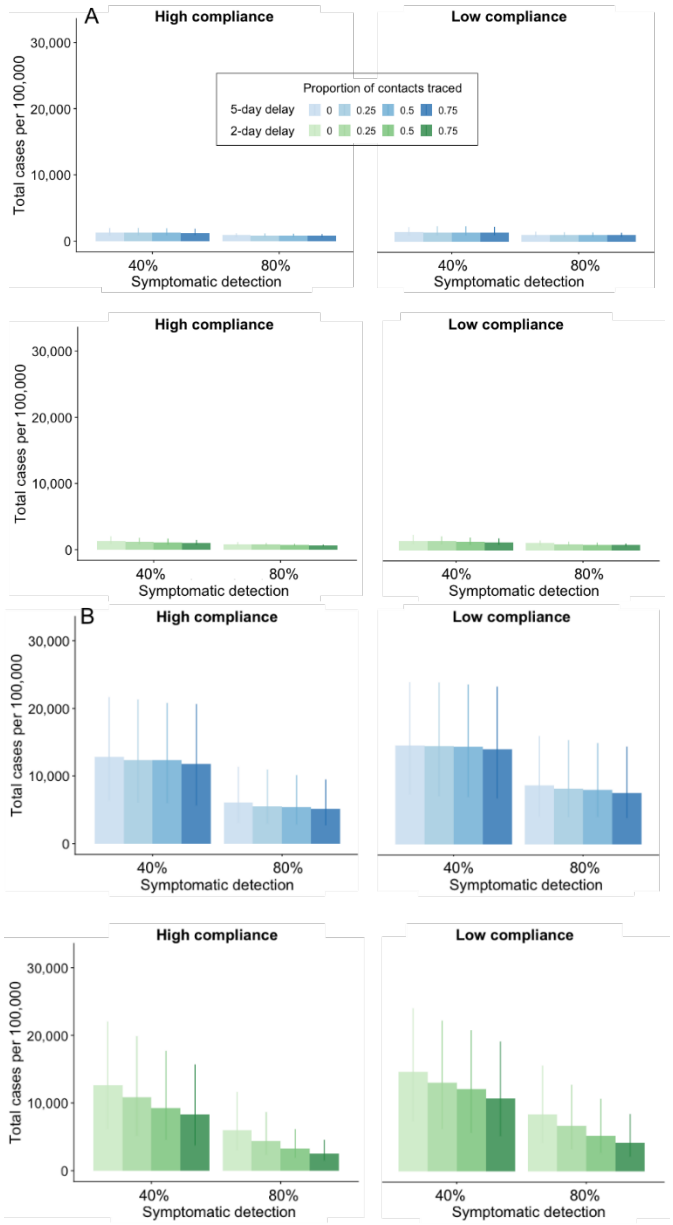

Figure S3.1. Sensitivity analysis with respect to compliance with isolation and quarantine. The graphs show the expected COVID-19 infections from November 8, 2020 to May 31, 2021, across a range of contact tracing scenarios with reproduction numbers of (A) R_0 = 0.95 and (B) R_0=1.2. Our primary analysis assumes a high level of compliance with isolation and quarantine, with contact reductions of 95% and 75%, respectively (left graphs). We compare this to lower contact reductions of 75% and 50%, respectively (right graphs). The sets of bars on x-axis correspond to the projected number of COVID-19 cases per 100,000 with 40% and 80% symptomatic case detection rates, assuming that detected cases seek a test two days after symptom onset and isolate at the time of specimen collection for the duration of their infectious period. Blue and green shading ranges from no contact tracing (light) to 75% of contacts isolated (dark) either five days (blue) or two days (green) after specimen collection from the index case. Bars and whiskers are medians and interquartile ranges from 200 stochastic simulations, respectively.

Sensitivity analysis with respect to asymptomatic ratio

Our base scenarios assume that 43% of infections are asymptomatic and that only symptomatic cases are tested and traced. Here we provide an alternate scenario where 25% infections are asymptomatic (36). The test-trace-isolate strategy has a higher impact if more infections are symptomatic. Assuming the same R_0 and given the increased infectiousness associated with symptomatic cases, testing and tracing would be expected to have a greater impact in the alternative than the baseline scenario. Specifically, we estimate a higher proportion of cases averted and a larger number of cases averted per case traced (Figure S3.2-S3.3).

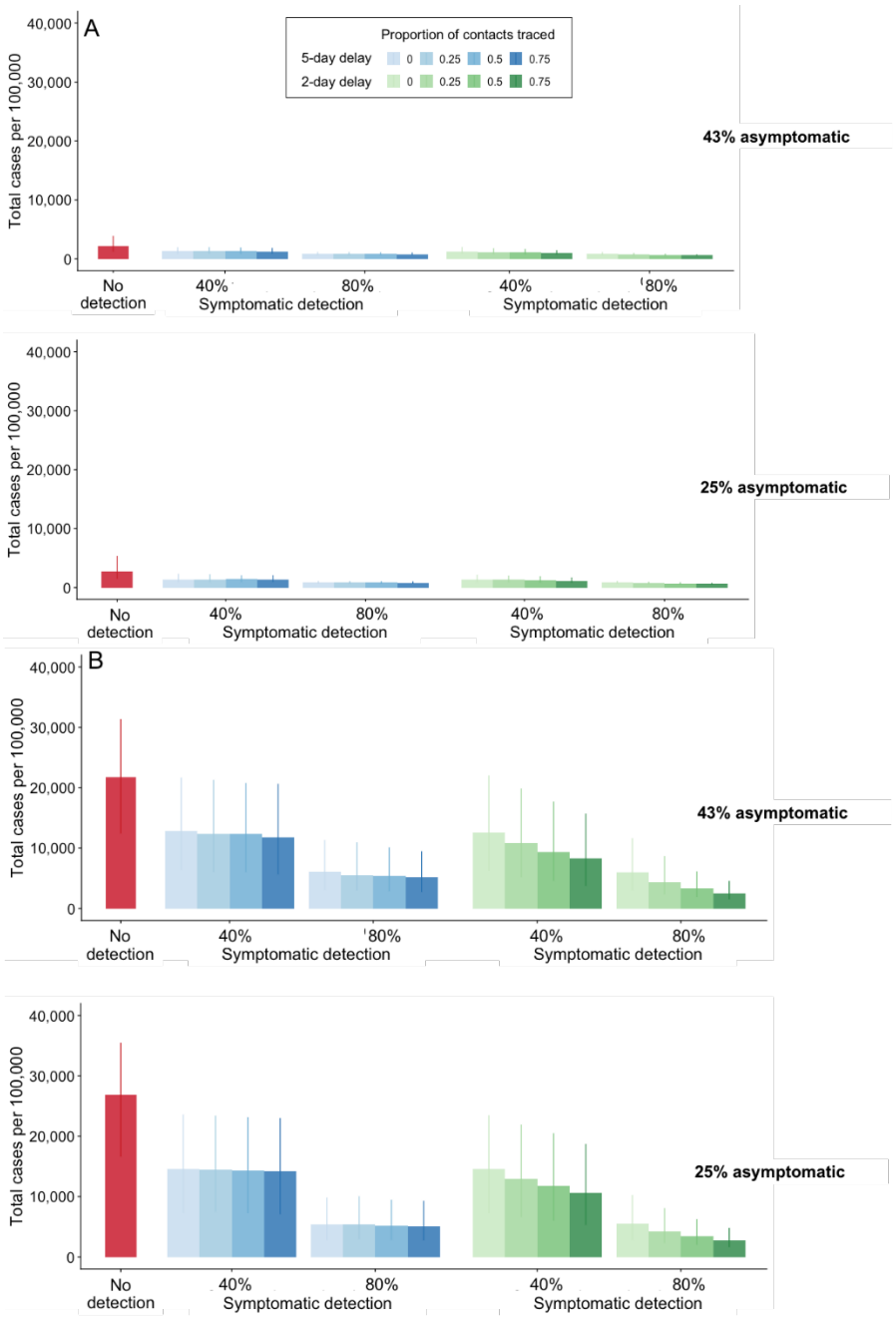

Figure S3.2. Expected COVID-19 attack rate from November 8, 2020 to May 31, 2021 across a range of case detection and proportion of contacts traced scenarios and reproduction numbers of (A) R_0 = 0.95 and (B) R_0=1.2. The top and bottom panels correspond to 43% and 25% asymptomatic ratio. Red bars represent the projected number of COVID-19 cases per 100,000 in the absence of testing. The left and right sets of blue bars correspond to 40% and 80% symptomatic case detection rates, respectively, assuming that detected cases seek a test two days after symptom onset and isolate at the time of specimen collection for the duration of their infectious period. Blue and green shading ranges from no contact tracing (light) to 75% of contacts isolated (dark) either five days (blue) or two days (green) after specimen collection from the index case. Bars and whiskers are medians and interquartile ranges from 200 stochastic simulations, respectively.

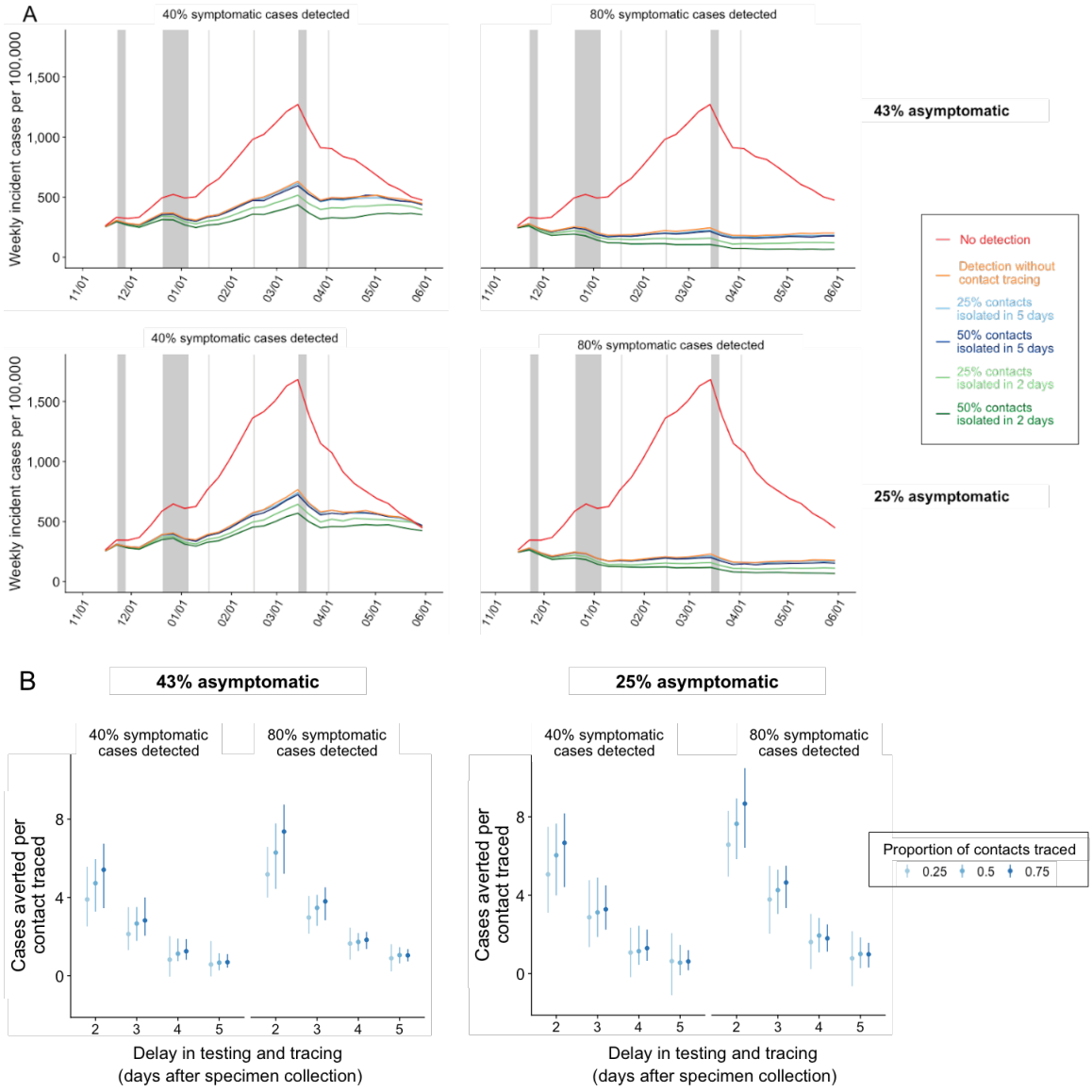

Figure S3.3. Expected COVID-19 incidence and cases averted per contact traced from November 8, 2020 to May 31, 2021 across a range of case detection and contact tracing scenarios, assuming R_0=1.2. A) Median estimated weekly incident COVID-19 cases across 200 stochastic simulations. Top and bottom panels assume 43% and 25% asymptomatic ratio. Red curves correspond to the no testing or tracing scenario. Left and right subpanels assume 40% and 80% of all symptomatics are detected and isolated, respectively. Orange curves correspond to testing without tracing; blue curves assume 25% or 50% of the contacts of the confirmed cases are traced and isolated five days after the isolation of the confirmed case; green curves assume 25% or 50% of the contacts of the confirmed cases are traced and isolated after two days. The gray vertical shading represents Thanksgiving break, winter break, and spring break for the local school district and the other vertical lines represent other school holidays including MLK, President's Day, and Easter (8). B) Number of COVID-19 cases averted per contact successfully traced as a function of lag from specimen collection from the index case to isolation of the contact. Left panel and right subpanels assume 40% and 80% of symptomatic cases are detected, respectively. The blue shading indicates 25%, 50%, or 75% of contacts successfully

traced. The points are medians from 200 paired stochastic simulations and the error bars are the interquartile ranges.

Additional figures with respect to hospitalizations and deaths

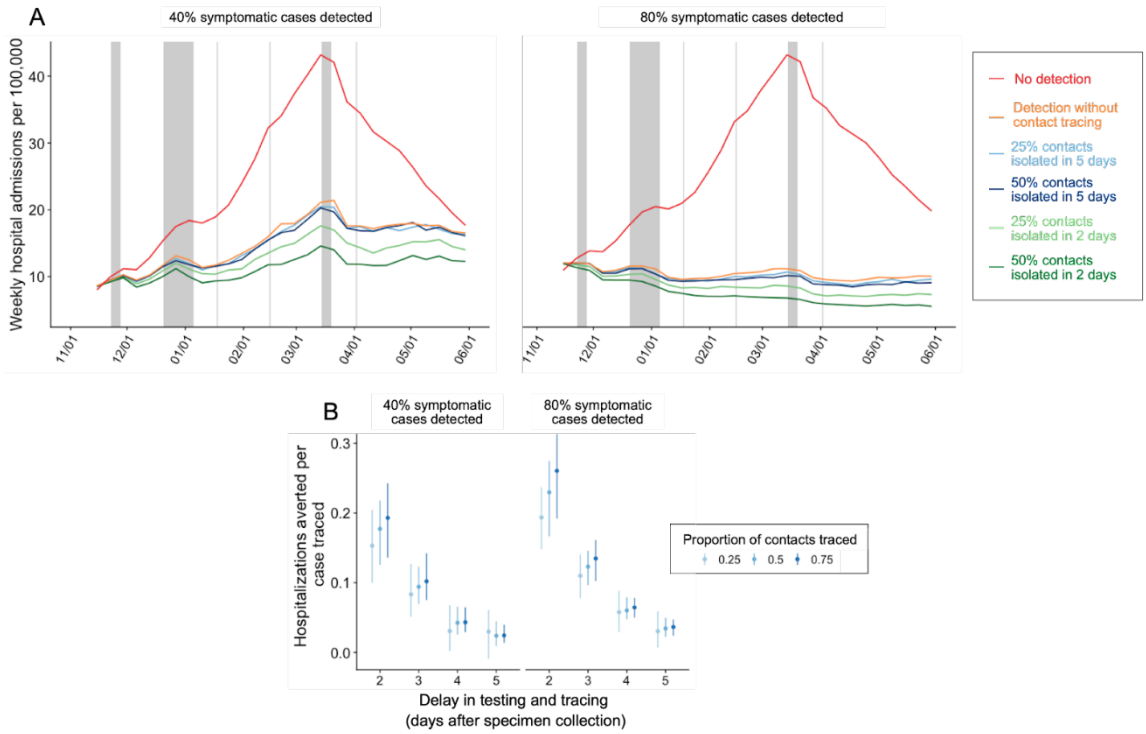

Figure S3.4. Expected COVID-19 hospitalizations and hospitalizations averted per contact traced from November 8, 2020 to May 31, 2021 across a range of case detection and contact tracing scenarios, assuming R_0=1.2. A) Median estimated weekly incident COVID-19 hospitalizations across 200 stochastic simulations. Top and bottom panels assume 43% and 25% asymptomatic ratio. Red curves correspond to the no testing or tracing scenario. Left and right subpanels assume 40% and 80% of all symptomatics are detected and isolated, respectively. Orange curves correspond to testing without tracing; blue curves assume 25% or 50% of the contacts of the confirmed cases are traced and isolated five days after the isolation of the confirmed case; green curves assume 25% or 50% of the contacts of the confirmed cases are traced and isolated after two days. The gray vertical shading represents Thanksgiving break, winter break, and spring break for the local school district and the other vertical lines represent other school holidays including MLK, President's Day, and Easter (8). B) Number of COVID-19 hospitalizations averted per contact successfully traced as a function of lag from specimen collection from the index case to isolation of the contact. Left panel and right subpanels assume 40% and 80% of symptomatic cases are detected, respectively. The blue shading indicates 25%, 50%, or 75% of contacts successfully traced. The points are medians from 200 paired stochastic simulations and the error bars are the interquartile ranges.

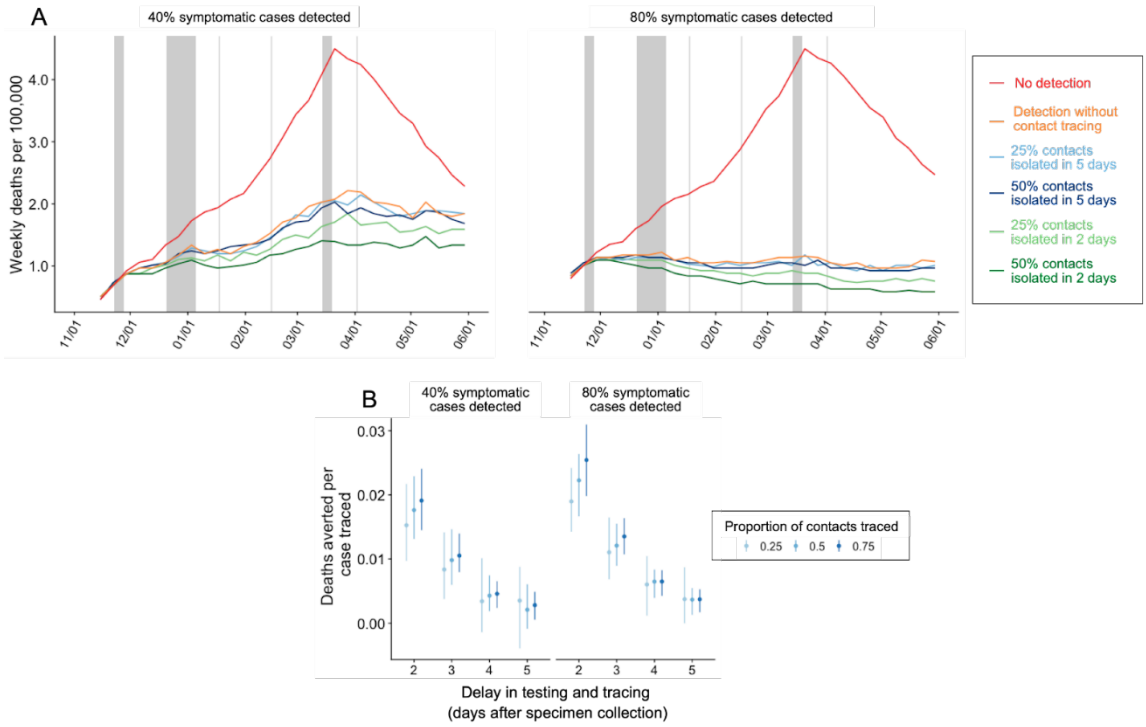

Figure S3.5. Expected COVID-19 deaths and deaths averted per contact traced from November 8, 2020 to May 31, 2021 across a range of case detection and contact tracing scenarios, assuming R_0=1.2. A) Median estimated weekly COVID-19 deaths across 200 stochastic simulations. Top and bottom panels assume 43% and 25% asymptomatic ratio. Red curves correspond to the no testing or tracing scenario. Left and right subpanels assume 40% and 80% of all symptomatics are detected and isolated, respectively. Orange curves correspond to testing without tracing; blue curves assume 25% or 50% of the contacts of the confirmed cases are traced and isolated five days after the isolation of the confirmed case; green curves assume 25% or 50% of the contacts of the confirmed cases are traced and isolated after two days. The gray vertical shading represents Thanksgiving break, winter break, and spring break for the local school district and the other vertical lines represent other school holidays including MLK, President's Day, and Easter (8). B) Number of COVID-19 deaths averted per contact successfully traced as a function of lag from specimen collection from the index case to isolation of the contact. Left panel and right subpanels assume 40% and 80% of symptomatic cases are detected, respectively. The blue shading indicates 25%, 50%, or 75% of contacts successfully traced. The points are medians from 200 paired stochastic simulations and the error bars are the interquartile ranges.

SI References

1. M. J. Keeling, P. Rohani, *Modeling Infectious Diseases in Humans and Animals* (Princeton University Press, 2011).
2. D. T. Gillespie, Approximate accelerated stochastic simulation of chemically reacting systems. *J. Chem. Phys.* 115, 1716–1733 (2001).
3. P. Ashcroft, *et al.*, COVID-19 infectivity profile correction. *Swiss Med. Wkly* 150, w20336 (2020).
4. Austin Dashboard (December 8, 2020).
5. S. Gao, J. Rao, Y. Kang, Y. Liang, J. Kruse, Mapping county-level mobility pattern changes in the United States in response to COVID-19. *arXiv [physics.soc-ph]* (2020).
6. A. A. King, D. Nguyen, E. L. Ionides, Statistical Inference for Partially Observed Markov Processes via the R Package pomp. *Journal of Statistical Software, Articles* 69, 1–43 (2016).
7. M. Tec, *et al.*, Austin COVID-19 transmission estimates and healthcare projections (February 5, 2021).
8. Calendar of Events. *Austin ISD* (March 26, 2020).
9. K. Prem, A. R. Cook, M. Jit, Projecting social contact matrices in 152 countries using contact surveys and demographic data. *PLoS Comput. Biol.* 13, e1005697 (2017).
10. J. Mossong, *et al.*, Social contacts and mixing patterns relevant to the spread of infectious diseases. *PLoS Med.* 5, e74 (2008).
11. O. Diekmann, J. A. P. Heesterbeek, M. G. Roberts, The construction of next-generation matrices for compartmental epidemic models. *J. R. Soc. Interface* 7, 873–885 (2010).
12. X. He, *et al.*, Temporal dynamics in viral shedding and transmissibility of COVID-19. *Nat. Med.* (2020) https:/doi.org/10.1038/s41591-020-0869-5.
13. D. F. Gudbjartsson, *et al.*, Spread of SARS-CoV-2 in the Icelandic Population. *N. Engl. J. Med.* (2020) https:/doi.org/10.1056/NEJMoa2006100.
14. Q. Bi, *et al.*, Insights into household transmission of SARS-CoV-2 from a population-based serological survey. *Nat. Commun.* 12, 3643 (2021).
15. R. Verity, *et al.*, Estimates of the severity of COVID-19 disease. *Epidemiology* (2020) https:/doi.org/10.1101/2020.03.09.20033357.
16. CDC, People at High Risk of Flu. *Centers for Disease Control and Prevention* (2019) (March 26, 2020).
17. CDC - BRFSS (2019) (March 26, 2020).
18. X. Zhang, *et al.*, Multilevel regression and poststratification for small-area estimation of population health outcomes: a case study of chronic obstructive pulmonary disease prevalence using the behavioral risk factor surveillance system. *Am. J. Epidemiol.* 179, 1025–1033 (2014).
19. S. Richardson, *et al.*, Presenting Characteristics, Comorbidities, and Outcomes Among 5700 Patients Hospitalized With COVID-19 in the New York City Area. *JAMA* 323, 2052–2059 (2020).
20. J. A. Lewnard, *et al.*, Incidence, clinical outcomes, and transmission dynamics of severe coronavirus disease 2019 in California and Washington: prospective cohort study. *BMJ* 369, m1923 (2020).
21. L. Tindale, *et al.*, Transmission interval estimates suggest pre-symptomatic spread of COVID-19. *Epidemiology* (2020) https:/doi.org/10.1101/2020.03.03.20029983.
22. 500 Cities Project: Local data for better health | Home page | CDC (2019) (March 19, 2020).
23. Health Outcomes | 500 Cities (2019) (March 28, 2020).
24. Part One: Who Lives with Chronic Conditions. *Pew Research Center: Internet, Science & Tech* (2013) (November 23, 2019).
25. C. for Disease Control, Prevention, Others, HIV surveillance report. 2016; 28. *URL: http://www. cdc. gov/hiv/library/reports/hiv-surveil-lance. html. Published November* (2017).
26. R. Sturm, A. Hattori, Morbid obesity rates continue to rise rapidly in the United States. *Int. J. Obes.* 37, 889–891 (2013).
27. O. W. Morgan, *et al.*, Morbid obesity as a risk factor for hospitalization and death due to 2009 pandemic influenza A(H1N1) disease. *PLoS One* 5, e9694 (2010).

28. Estimating the Number of Pregnant Women in a Geographic Area from CDC Division of Reproductive Health.
29. G. F. Miller, E. Coffield, Z. Leroy, R. Wallin, Prevalence and Costs of Five Chronic Conditions in Children. *J. Sch. Nurs.* 32, 357–364 (2016).
30. Cancer Facts & Figures 2014 (March 30, 2020).
31. C. M. Hales, C. D. Fryar, M. D. Carroll, D. S. Freedman, C. L. Ogden, Trends in Obesity and Severe Obesity Prevalence in US Youth and Adults by Sex and Age, 2007-2008 to 2015-2016. *JAMA* 319, 1723–1725 (2018).
32. R. K. Zimmerman, D. S. Lauderdale, S. M. Tan, D. K. Wagener, Prevalence of high-risk indications for influenza vaccine varies by age, race, and income. *Vaccine* 28, 6470–6477 (2010).
33. J. A. Martin, B. E. Hamilton, M. J. K. Osterman, A. K. Driscoll, P. Drake, Births: Final Data for 2017. *Natl. Vital Stat. Rep.* 67, 1–50 (2018).
34. T. C. Jatlaoui, *et al.*, Abortion Surveillance - United States, 2015. *MMWR Surveill. Summ.* 67, 1–45 (2018).
35. S. J. Ventura, S. C. Curtin, J. C. Abma, S. K. Henshaw, Estimated pregnancy rates and rates of pregnancy outcomes for the United States, 1990-2008. *Natl. Vital Stat. Rep.* 60, 1–21 (2012).
36. A. Aleta, *et al.*, Modelling the impact of testing, contact tracing and household quarantine on second waves of COVID-19. *Nat Hum Behav* 4, 964–971 (2020).